Computational study of helix wave formation in active media

Petteri Kettunen [a] Paul D. Bourke [b] Hajime Hashimoto [c]

Takashi Amemiya [d] Stefan C. Müller [e] Tomohiko Yamaguchi [a,f,*]

[a] *Nanotechnology Research Institute, National Institute of Advanced Industrial Science and Technology, AIST Central 5–2, Higashi 1–1–1, Tsukuba, Ibaraki 305–8565, Japan*

[b] *Astrophysics and Supercomputing, Swinburne University of Technology, P.O. Box 218, Hawthorn, Victoria 3122, Australia*

[c] *Ube National College of Technology, Department of Electrical Engineering, Tokiwadai 2–14–1, Ube 755–8555, Japan*

[d] *Graduate School of Environment and Information Sciences, Yokohama National University, 79–7 Tokiwadai, Hodogaya–ku, Yokohama 240–8501, Japan*

[e] *Institut für Experimentelle Physik, Otto-von-Guericke-Universität Magdeburg, Universitätsplatz 2, D-39106 Magdeburg, Germany*

[f] *Graduate School of Pure and Applied Science, University of Tsukuba, 1-1-1 Tennoudai, Tsukuba 305-8577, Japan*

Abstract

Computer simulations of excitation wave formation in a three–dimensional Belousov–Zhabotinsky reaction medium is presented. The modelled system is an elongated domain with immobilised catalyst connected to an ideal reservoir of reactants. It is shown that transient spatial inhomogeneities within the reactant diffusion coupled

with oscillatory reaction kinetics give rise to helical waves. Good agreement with prior experimental observations is obtained and these simulations provide a proof of formation of helicoidal dissipative structures under macroscopically unperturbed conditions.

Key words: Belousov–Zhabotinsky reaction, dissipative structures

1 INTRODUCTION

Transmission of propagating excitation waves is observed and studied in various biological and nonlinear reaction–diffusion systems, such as the aggregation process of *Dictyostelium discoideum* cells and the slugs [1], Ca^{2+} waves in the cytoplasm of *Xenopus laevis* oocytes [2], CO oxidation on Pt(110) surface [3], and the Belousov–Zhabotinsky reaction (BZR) [4]. These excitation waves are not always symmetrical (i.e., concentric rings) but can be characterised by spirals rotating in clockwise or counter-clockwise direction. This symmetry-broken structure can be induced artificially by external perturbation, typically by applying share stress or introducing obstacles against wave propagations in aqueous BZR, or by light irradiation to erase a part of wave fronts in the photo–sensitive BZR [5]. In a catalyst–immobilised gel system, on the other hand, two–dimensional (2D) spirals [6] and three–dimensional (3D) rotors (helices) [7] emerge occasionally and spontaneously in the course of diffusion of reactants into the gel. 3D structures of the BZR rotors in laboratory experiments have been reconstructed using optical tomography [8,9], and theoretical bases for describing the dynamics and time evolution of twisted scroll waves

* Author to whom correspondence should be addressed.

have been proposed [10–12]. It is also known that there exists a 3D rotor observable as a coherent cell motion in a leading part of slug of *Dictyostelium discoideum* [13] which is considered to be responsible for the polarity of slug and subsequent cell differentiation. The origin as well as properties and dynamics of 3D rotors are of particular interest in cardiac electro–physiology where rotating wave segments are precursors of fatal ventricular fibrillation [14–16].

This study presents computational results on autonomous helicoidal wave formation in a 3D BZR. We use a model of 3D reaction medium resembling a catalyst–immobilised gel in a capillary glass tube. One end of the medium is open to an ideal reservoir of reactants (the other components of BZR except the catalyst) while the other boundaries are non–flux Neumann type. As the system changes from inactive to active due to reactant diffusion, we observe formation of dynamic spatio-temporal dissipative structures. The results described here contain issues of symmetry-breaking that are not induced by external control. The model employed is derived from nonlinear reaction kinetics with linear diffusion terms.

2 NUMERICAL MODEL

The reaction–diffusion model is based on the Tyson–Fife scaling of the two–variable Oregonator [17–19] modified to account for the diffusion of reactants [20]. The three-variable system is given by

$$\frac{\partial u}{\partial \tau} = \nabla^2 u + \frac{1}{\epsilon}\left(\hat{u} - \hat{u}^2 - f\,v\,\frac{\hat{u}-q}{\hat{u}+q}\right) \ , \tag{1}$$

$$\frac{\partial v}{\partial \tau} = \hat{u} - v \ , \tag{2}$$

$$\frac{\partial r}{\partial \tau} = \nabla^2 r \ , \tag{3}$$

where u and v describe the concentrations of $HBrO_2$ (activator) and oxidised catalyst (inhibitor), respectively; r is a normalised ($0 \leq r \leq 1$) dimensionless variable describing spatiotemporal reactant concentration and $\nabla^2 = \frac{\partial^2}{\partial x^2} + \frac{\partial^2}{\partial y^2} + \frac{\partial^2}{\partial z^2}$ is the 3D Laplacian operator. Terms ϵ, q, and f are the parameters of the Tyson–Fife model [18,19] and the linear coupling of excitability and reaction dynamics is modelled using [20]

$$\hat{u} = u \cdot r. \tag{4}$$

We set the cartesian coordinate system so that the long axis is along z–direction and the boundary connecting to the reactant reservoir is at $z = 0$. In order to simulate the initial random diffusion process, which corresponds to the roughness the of gel surface in the laboratory experiments [7], we introduce the following 3D–boundary conditions. (1) Any grid site at $z = 0$ is an open site for diffusion with probability p and a closed site with probability $1 - p$. (2) An open site extends into the medium in z-direction a random length (uniform deviate) of maximum L_p grid sites (Fig. 1). (3) Initially the closed sites are set to value $r_{min} = 0$ whereas the open sites are kept constant as $r_{max} = 1$ [20]. Any initial condition with at least one open site renders the asymptotic solution of Eqs. (1)–(4) to that of the original two–variable Oregonator model.

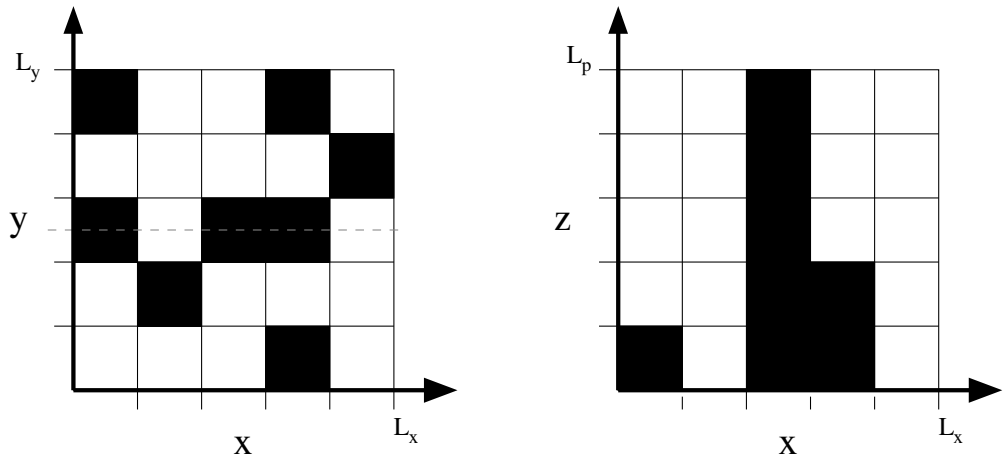

Fig. 1. Schematics of the model of open and closed sites at the boundary of reactant reservoir ($z = 0$) and reaction medium ($z > 0$). Panel on the left shows grid (x, y) plane at $z = 0$. Open and closed sites are indicated by black and white squares, respectively. Graph on the right presents how open sites penetrate into the reaction medium along the gray dashed line on the left. In this example illustration $L_x = L_y = L_p = 5$.

3 SIMULATIONS

After initial simulations it became evident that visualisation of the resulting 3D data presents a problem on its own. Isosurface rendering [21] with appropriate threshold value extracted typically two surfaces close to each other. If the surface is visualised using opaque graphic primitives (e.g. triangles or tetrahedrons) and only one viewpoint is used, it hinders further the perceived information of 3D wave structure. Therefore a volumetric representation of the simulation data was created by mapping the values of u to opacity and colour (Fig. 2), which is then rendered using ray tracing [22]. This technique does not require any implicit knowledge on characteristics of the BZR excitation waves and produces high–quality visualisations even from relatively coarse grids.

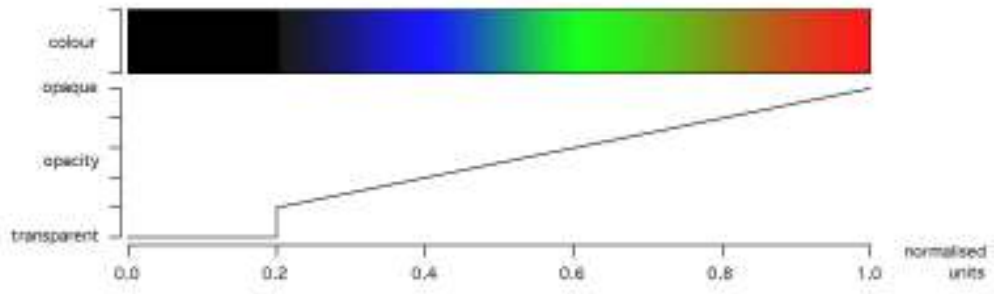

Fig. 2. Opacity and colour mapping used in volume rendering of 3D voxel data For example, those parts of the volume with u less than 0.2 are totally transparent but voxels become increasingly opaque as u increases. A standard red-green-blue colour ramp is employed to colour the voxels, again as a linear function of u.

Figure 3A shows a snapshot of a selected simulation which exhibited non–trivial pattern formation. In the early stages there is an autonomously formed wave segment, a rotor, rotating counter–clockwise within the diffusion domain open to the reactant reservoir. Because of the limitation of the diffusing amount of reactant at this phase, the excitable medium and consequently the wave is effectively two–dimensional. Given more time for reactant diffusion to enlarge the excitable domain, one can see signs of 3D spatial effects inducing distinctive changes in wave fronts in the less–exitable area (Fig. 3B). The waves emitted by the rotating vortex extend out in space along the long z-axis and become planar waves which propagate away from the rotor. These planar waves disappear when they reach the area which is not yet capable of supporting wave propagation. However, the 3D wave keeps rotating in a stable self–sustaining manner and penetrates deeper into the medium. Once reactants have reached the other end of the medium (but the system is not yet completely saturated), an intermediate transient state can be characterised. The space ca. 55% in the left is dominated by rotating helicoidal structure and

the rest by propagating planar waves (Fig. 3C). This hybrid state evolves then into fully helicoidal structure which extends itself completely throughout the long axis (Figs. 3D–E). The rotor's rotation time observed from (x, y) plane was $\tau \approx 2.65$ and it remained constant throughout the simulation.

Figure 4 shows graphs depicting the dynamic evolution of filament shape in 3D space after the helix wave has stabilised completely end–to–end along the long axis. Here the filament is defined as a line–trace along the z–axis of the singular point (i.e. the tip) of 2D spiral of each (x, y)–plane. By denoting $L = L_x = L_y$, dynamics can be summarised with: (1) one and half twists and large cylindrical core (radius $\approx L/3$, Figs. 4A–B) (2) one full twist, core radius $\approx L/4$ (Fig. 4C) (3) one and half twists, core radius $\approx L/6$ (Fig. 4D). Thus, the core radius tended to become smaller with reactant saturation, and the filament to become straight to decrease its length. Eventually the filament broke due to the interaction with boundaries (data not shown) but continuous form was nevertheless re–established. However, this induced additional twist into filament shape and enlarged the core radius (Fig. 4E). Additionally the filament is prominently straight in space 25%–30% on the left during its early development (Figs. 4A–B). This phenomenon was observed in experiments as well [7].

Results from further simulations carried out to determine the effect of excitability (stoichiometric parameter f) on the formation of singular filaments in the reservoir–reaction medium boundary are shown in Fig. 5. There is a window in parameter range from $f \approx 1.2$ to $f \approx 1.8$ within which the rotors are optimally formed and the maximum probability is obtained at $f \approx 1.4$. This suggests that excitability has a modest yet observable relation to the probability with which helix waves can occur. Qualitatively this confirms re-

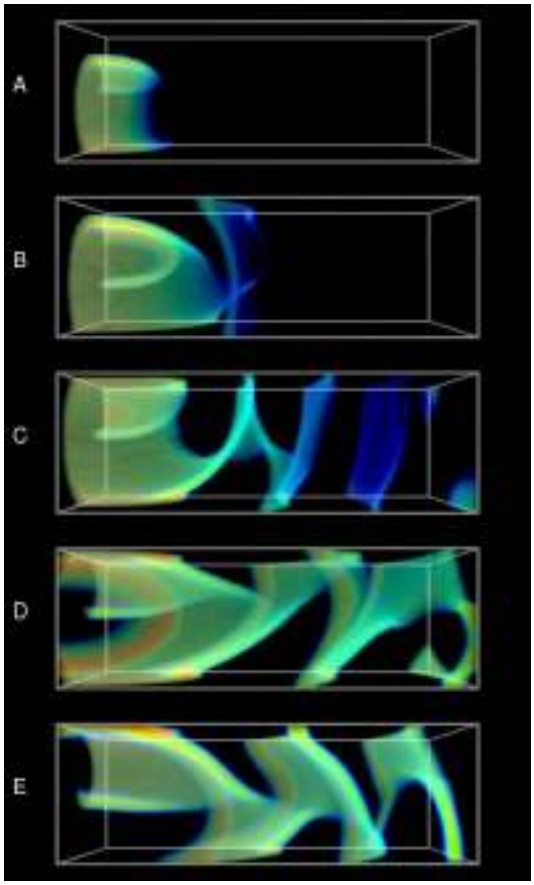

Fig. 3. Volume renders of variable u using opacity and colour mappings shown in Fig. 2. Data was collected at $\tau = 1667$ (A), $\tau = 2667$ (B), $\tau = 3167$ (C), $\tau = 13000$ (D) and $\tau = 241000$ (E). Eqs. (1)–(4) was integrated on a 3D rectangular grid ($z = 0$, left) with the forward Euler method using the standard seven–point approximation for the 3D Laplacian operator [23]. Parameters: $\epsilon = 0.02$, $q = 0.002$, $f = 1.25$, grid size $N_x \times N_y \times N_z = 32 \times 32 \times 96$, grid spacing $\Delta = 1/2$, time step $\delta\tau = 3.333 \cdot 10^{-3}$, $p = 0.13$, $L_p = 13$ (p and L_p were chosen empirically). Decreasing the time step by factor of two did not alter the simulated behavior. These simulations were carried on a GNU/Linux workstation with 1.3 MHz Intel Celeron CPU and 512 MB of RAM. Effective performance was 41.7 iterations per second in integration and ca. 150 seconds in ray–tracing a single 600×600 image from volumetric data.

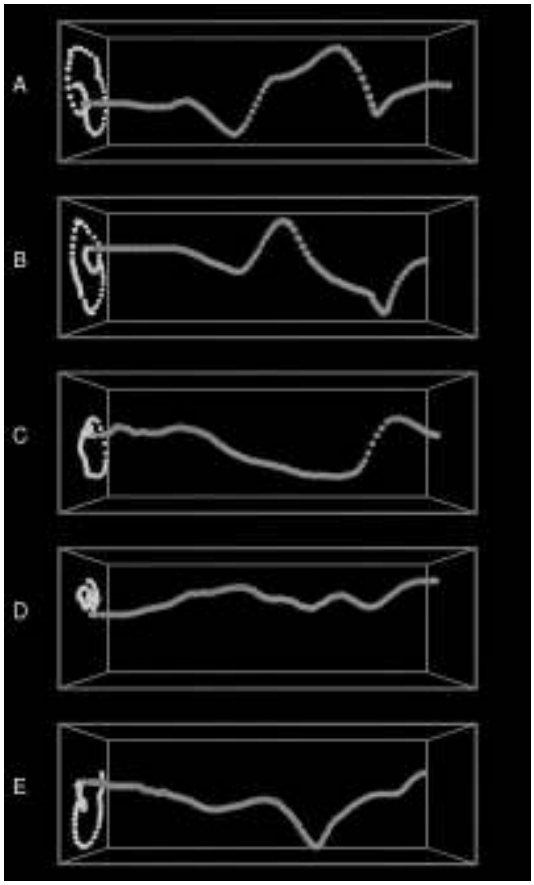

Fig. 4. 3D visualisations of singular filament with its (x, y) positions projected onto a single plane at $z = 0$. Time in each panel is $\tau = 3333$ (A), $\tau = 8333$ (B), $\tau = 45000$ (C), $\tau = 293000$ (D) and $\tau = 326333$ (E). Filament position was obtained by extracting normalised monochrome image from variable u ($N_x \times N_y$ pixels, one byte per pixel) for each z. These images were subjected to threshold at 200 by mapping pixels below that to 0 (black) and rest to 255 (white). Then Laplacian kernel was calculated to each pixel, omitting the border pixels, with weight 8 to the center pixel and weights 1 to neighbour and next nearest neighbour pixels. Filament location was in the position where Laplacian field was at minimum. Typical maximum error rate using this method was less than 6%. After visual corrections data was smoothed using five–point moving average.

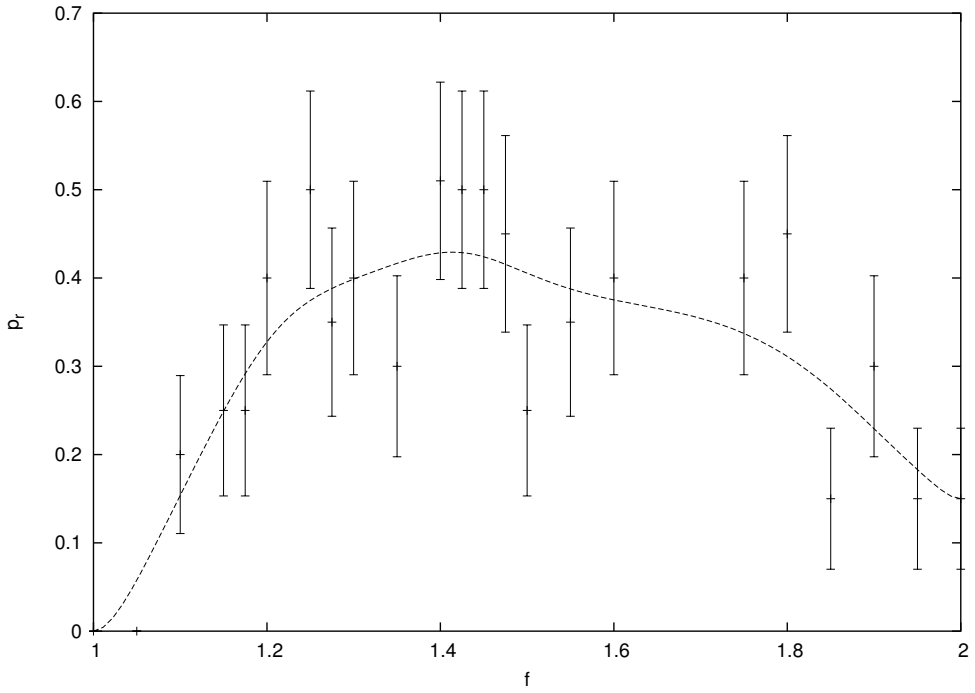

Fig. 5. Probability of rotor formation p_r (with standard error) in the open boundary as a function of excitability f and its fitted curve approximation (dashed line). Model and numerical parameters, except f, are as in Fig. 3.

sults obtained in similar 2D simulations [20].

4 DISCUSSION

Our calculations demonstrate that complex dissipative structures can evolve autonomously in a simplistic unperturbed systems. The trigger for formation of rotors (i.e., symmetry-broken structures), and of a succeeding train of planar waves, comes from a realistic model of inhomogeneous diffusion of reactants into homogeneous reaction media. It should be stressed that this is strictly an initial–value problem. A study conducted by Steinbock *et al.* found qualitatively similar modes of wave propagation in modelling *Dictyostelium* mor-

phogenesis but they relied on explicitly inducing discontinuities into spatial excitability properties [24]. In this present study, linear diffusion and continuous concentration gradient are key elements in evolution and survival of the helix wave. When the initial rotor emerges, the excitable space is effectively 2D and its expansion in z–direction is slow due to a large concentration gradient of reactants. This provides the rotating wave segment an optimal domain to suppress competing oscillations and to stabilise itself. Once the medium becomes sufficiently saturated and transition from effectively 2D to 3D begins, the rotor has already reached a self–sustaining state. This rotor becomes then the pivot structure from which filament extends itself into 3D space. Interestingly, this type of 2D–3D transition of reaction medium is known to induce changes which may lead to wave breakup and turbulence [5,16].

Our simulations on helix–filament formation verify theoretical predictions by Panfilov *et al.* [25] and findings in real chemical [7] and biological [13,26] media. The results also provide argument that formation of spiral–type vortices does not necessarily require macroscopic perturbations of control parameters in active media. Rather, alterations in spatial diffusive properties at microscopic level can induce phase shift of oscillating ensembles. Consequently, this can lead to spiral formation in 2D [20] or helix waves in 3D as is shown here. Relevant analogical counterpart to the 3D BZR in biology is cardiac [27,28] or neuronal tissue [29]. Following the present results, diffusion properties of active species or reactants in such systems can initiate onset of disturbing anomalies even though reaction media as such is capable of conducting normal metabolism.

Acknowledgements

This research was partly supported by the Shorai Foundation and the Japan Science and Technology Agency (JST), CREST.

References

[1] G. Gerisch. Periodische Signale steuern die Musterbildung in Zellbänden. *Naturwissenschaften*, 58:430–438, 1971.

[2] J. Lechleiter, S. Girard, E. Peralta, and D. Clapman. Spiral calcium wave propagation and annihilation in xenopus laevis oocytes. *Science*, 252:123–126, 1991.

[3] R. Imbihl and G. Ertl. Oscillatory kinetics in heterogeneous catalysis. *Chem. Rev.*, 95:697–733, 1995.

[4] R. Kapral and K. Showalter, editors. *Chemical Waves and Patterns*. Kluwer, Dordrecht, Netherlands, 1995.

[5] T. Amemiya, S. Kádár, P. Kettunen, and K. Showalter. Spiral wave formation in three–dimensional excitable media. *Phys. Rev. Lett.*, 77:3244–3247, 1996.

[6] T. Yamaguchi, L. Kuhnert, Zs. Nagy-Ungvarai, S.C. Müller, and B. Hess. Gel systems for the Belousov–Zhabotinskii reaction. *J. Phys. Chem.*, 95:5831–5837, 1991.

[7] T. Yamaguchi and S.C. Müller. Front geometries of chemical waves under anisotropic conditions. *Physica D*, 49:40–46, 1991.

[8] A.T. Winfree, S. Caudle, G. Chen, P. McGuire, and Z. Szilagyi. Quantitative optical tomography of chemical waves and their organizing centers. *Chaos*, 6:617–626, 1996.

[9] U. Storb, C.R. Neto, M. Bär, and S.C. Müller. A tomographic study of desynchronization and complex dynamics of scroll waves in an excitable chemical reaction with a gradient. *Phys. Chem. Chem. Phys.*, 5:2344–2353, 2003.

[10] J.P. Keener. The dynamics of three dimensional scroll waves in excitable media. *Physica D*, 31:269–276, 1988.

[11] J. P. Keener and J. J. Tyson. Helical and circular scroll wave filaments. *Physica D*, 44:191–202, 1990.

[12] J. P. Keener and J. J. Tyson. The dynamics of helical scroll waves in excitable media. *Physica D*, 53:151–161, 1991.

[13] F. Siegert and C.J. Weijer. Digital image processing of optical density wave propagation in dictyostelium discoideum and analysis of the effects of caffeine and ammonia. *J. Cell Sci.*, 93:325–335, 1989.

[14] R.A. Gray, A.M. Pertsov, and J. Jalife. Spatial and temporal organization during cardiac fibrillation. *Nature*, 392:75–78, 1998.

[15] F. Witkowski, F.X. Leon, P.A. Penkoske, W.R. Gilse, M.L. Spano, W.L. Ditto, and A.T. Winfree. Spatiotemporal evolution of ventricular fibrillation. *Nature*, 392:78–82, 1998.

[16] M.-H. Lee, Z. Qu, G.A. Fishbein, S.T. Lamp, E.H. Chang, T. Ohara, O. Voroshilovsky, J.R. Kil, A.R. Hamzei, N.C. Wang, S.-F. Lin, J.N. Weiss, A. Garfinkel, H.S. Karagueuzian, and P.S. Chen. Patterns of wave break during ventricular fibrillation in isolated swine right ventricle. *Am. J. Physiol. Heart Circ. Physiol.*, 281(1):H253–265, 2001.

[17] R.J. Field and R.M. Noyes. Oscillations in chemical systems IV: Limit cycle behavior in a model of a real chemical reaction. *J. Chem. Phys*, 60:1877–1884, 1974.

[18] J.J. Tyson and P.C. Fife. Target patterns in a realistic model of the Belousov–Zhabotinskii reaction. *J. Phys. Chem.*, 73:2224–2237, 1980.

[19] J.P. Keener and J.J. Tyson. Spiral waves in the Belousov–Zhabotinskii reaction. *Physica D*, 21:307–324, 1986.

[20] P. Kettunen, T. Amemiya, T. Ohmori, and T. Yamaguchi. Spontaneous spiral formation in two–dimensional oscillatory media. *Phys. Rev. E*, 60:1512–1515, 1999.

[21] W.E. Lorensen and H.E. Cline. Marching cubes: a high resolution 3d surface reconstruction algorithm. *Computer Graphics*, 21(4):163–169, 1987.

[22] M. Levoy. Efficient ray tracing of volume data. *ACM Transactions on Graphics*, 9(3):245–261, 1990.

[23] W.H. Press, B.P. Flannery, S.A. Teukolsky, and W.T. Vetterling. *Numerical Recipes in C.* Cambridge University Press, New York, 1992.

[24] O. Steinbock, F. Siegert, S.C. Müller, and C.J. Weijer. Three–dimensional waves of excitation during Dictyostelium morphogenesis. *Proc. Natl. Acad. Sci. USA*, 90:7332–7335, 1993.

[25] A.V. Panfilov, A.N. Rudenko, and A.M. Pertsov. Twisted scroll waves in three-dimensional active media. In V.I. Krinsky, editor, *Self Organization – Autowaves and Structures far from Equilibrium*, pages 103–105. Springer, Berlin, 1984.

[26] F. Siegert and C.J. Weijer. Three–dimensional scroll waves organize Dictyostelium slugs. *Proc. Natl. Acad. Sci. USA*, 89:6433–6437, 1992.

[27] J.M. Davidenko, A.V. Pertsov, R. Salomonsz, W. Baxter, and J. Jalife. Stationary and drifting waves of excitation in isolated cardiac muscle. *Nature*, 355:349–351, 1992.

[28] J.P. Keener and A.V. Panfilov. Three dimensional propagation in the heart: The effects of geometry and fiber orientation on propagation in myocardium. In D.P. Zipes and J. Jalife, editors, *Cardiac Electrophysiology*, pages 335–348. W.B. Saunders Company, Darien, 1995.

[29] O.E. Rössler. in Physics and Mathematics of the Nervous System, M. Conrad, W. Güttinger, M. Dal Cin (Eds), 1974.